This is a provisional PDF only. Copyedited and fully formatted version will be made available soon.

Computational modeling of the cephalic arch with jugulocephalic vein variant predicts hemodynamic profiles in patients with brachiocephalic fistula

Authors: Jiaoran Li, Junrui Chen, Xuetao Zhu, Kaining Huo, Xianhao Shao, Menglin Cong, Zhen Liu, Zhenzhong Li, Weiming Yue

Computational modeling of the cephalic arch with jugulocephalic vein variant predicts hemodynamic profiles in patients with brachiocephalic fistula

Jiaoran Li et al., Computational hemodynamic model of cephalic vein variant

Jiaoran Li[1], Junrui Chen[2], Xuetao Zhu[3], Kaining Huo[4], Xianhao Shao[5], Menglin Cong[3], Zhen Liu[4], Zhenzhong Li[4], Weiming Yue[1]

[1]Department of Thoracic Surgery, Qilu Hospital, Shandong University, Jinan, Shandong Province, China

[2]Department of Marine Engineering, Haerbin Institute of Technology, Weihai, Shandong Province, China

[3]Department of Orthopaedics, Qilu Hospital, Shandong University, Jinan, Shandong Province, China

[4]Department of Anatomy and Neurobiology, School of Basic Medical Sciences, Shandong University, Jinan, Shandong Province, China

[5]Department of Orthopaedics, Shandong Provincial Hospital Affiliated to Shandong First Medical University, Jinan, Shandong, China

Address for correspondence: Weiming Yue, Department of Thoracic Surgery, Qilu Hospital, Shandong University, 107 Wenhua Xi Road, Jinan, Shandong Province, 250012, China, tel: +86 185 6008 6960, e-mail: ywmfz2013@126.com

Abstract

Background: The cephalic vein is often used in for arteriovenous fistula creation; however, the cephalic vein variation is common. This study will propose new theoretical explanations for a new discovered variation of cephalic vein draining into external jugular vein with "T-junction" shape by means of 3D computational hemodynamic modeling, which may provide reference for clinical practice.

Methods: The precise measurements were conducted for the variant right cephalic vein draining into external jugular vein and for a normal right cephalic vein as a

control. After processing the anatomical data, 3D geometrical model was reconstructed. Then, the influent field inside the variant jugulocephalic vein was mathematically modeled to get a detailed description of hemodynamic environment.

Results: The anatomical parameters of the "T-junction" jugulocephalic vein variant were much more different from the normal right cephalic vein. The wall shear stress of variant cephalic vein at the corresponding position was higher and changed more rapidly than that of normal cephalic vein. The shear rate contour lines are disordered in several areas of the variant cephalic vein, indicating that the hemodynamic parameters in these areas are unstable. The hemodynamic characteristics at the confluence of the variant cephalic vein are more complex, with more areas where hemodynamic parameters are disrupted.

Conclusions: The variation of cephalic arch in a "T-junction" with external jugular vein largely altered the fluid dynamics, especially in hemodialysis patients with brachiocephalic fistula in terms of the simulating flow in 3D computational model. This computational model provides hemodynamic profiles for stabilizing or modulating fluid dynamics in patients with jugulocephalic vein variant after brachiocephalic fistula.

Keywords: computational modeling, jugulocephalic vein variant, cephalic arch, brachiocephalic fistula, hemodynamics

INTRODUCTION

The cephalic vein is superficial and the course is constant in the arm. It is often used for arteriovenous fistula creation. Variations in the cephalic vein are common in clinical cases [14]. The variant cephalic vein may affect normal surgical procedures. Hence, anatomical variation of cephalic vein is of clinical and surgical significance, and healthcare professionals must be aware of the variation of this vessel [2]. Here, we found a rare anatomic variant of a single-conduit supraclavicular cephalic arch draining into the external jugular vein. The venous blood drainage in this variant cephalic arch may not be problematic in vivo under physiological conditions [12].

However, in disease conditions, such as brachiocephalic fistula, the blood pressure and hemodynamics in this variant cephalic arch may change dramatically, which related to the adverse effects on patients [4]. There is a case report of a patient with similar cephalic vein variation who underwent brachiocephalic fistula [11]. The first stenosis of variant cephalic vein was dilated with a balloon. After that, the stenoses presented with recurrent in cephalic arch. This phenomenon indicates that stenosis is more likely to occur in this variant condition. However, the mechanism of fistula stenosis in this variant cephalic vein should be further analyzed in order to provide a reasonable theoretical explanation for the recurrent stenosis and provide valuable reference in clinical practice. Therefore, we try to use 3D computational hemodynamic modeling to simulate the in vivo states of the single-conduit supraclavicular cephalic arch draining into the external jugular vein variant and predict adverse effects due to abnormal hemodynamic changes after brachiocephalic fistula.

Computational fluid dynamics (CFD) uses numerical methods for calculating physical parameters to simulating the hemodynamic environment based on real-world flow field. Changes in the hemodynamic environment can alter the stress on vascular endothelial cells, which is an important mechanism for the pathogenesis of many vascular diseases[20]. CFD models can simulate hemodynamic changes in various vascular disease states. With the advancement of computational sciences and technique, CFD tools can be used to simulate hemodynamic parameters such as fluid flow velocity, pressure, and wall shear stress at any point of the model, more accurately explaining the pathological process of the disease. Currently, it is mostly used in fields such as coronary heart disease and cerebrovascular diseases [23]. CFD tools have been used to investigate the pathological basis of arteriovenous fistula maturation and stenosis [19]. In our present study, CFD was used for imitating hemodynamic alterations in anatomical variation. Although using 3D computational hemodynamic models to simulate the blood flow in normal and variant states in vivo can not fully explain the mechanism of stenosis in this variant cephalic arch after

brachiocephalic fistula, the computational simulation data of the present study will usher us for better understanding of the occurrence and development of the hemodynamic abnormalities.

We raised several concerning scientific questions based on this specific "T-junction" single-conduit supraclavicular cephalic arch draining into the external jugular vein underwent brachiocephalic fistula: (1) the features of the hemodynamic abnormalities during maturation; (2) the theoretical reasons of stenosis and maturation failure; (3) the existence of the risk after stenosis. This study will propose new theoretical explanations for the above-mentioned questions by means of 3D computational hemodynamic modeling, provide reference for clinical practice, and point out the research direction for further in-depth study on the mechanism of hemodynamic changes and the deep-seated causes of the stenosis in this specific "T-junction" single-conduit supraclavicular cephalic arch draining into the external jugular vein.

MATERIALS AND METHODS

Discovery of a jugulocephalic vein variant

A variation of a "T-junction" single-conduit supraclavicular cephalic arch draining into the external jugular vein was found in a male embalmed cadaver (body height 173 cm) during routine dissection.

The variant cephalic vein has abnormal routing and drainage. The diameter of this variant cephalic vein is quite smaller than the normal cephalic vein, and the variant vein routed lateral to deltopectoral groove. Instead of penetrating clavipectoral fascia, the variant cephalic arch went superficial to clavicle and drained into external jugular vein.

The measurement of parameters of right cephalic arch variation

Based on anatomical morphology of cephalic vein, clinical operation process of arteriovenous fistula creation, theoretical and practical purpose of computational modeling, our present computational fluid model intends to collect anatomical data of

normal and variant cephalic vein, which begin from the midpoint of the arm: (1) It is conducive to defining vascular segment and measuring anatomical parameters, so that we can conduct 3D simulation of both normal and variant cephalic vein for comparative investigation. (2) We defined the inlet of computational fluid model at the midpoint of the arm for preventing the interference of the disturbed blood flow near the anastomosis, so the blood flow around the computational fluid inlet was regarded as laminar flow. (3) Since the curved segment has both theoretical and practical significance for hemodynamic modeling, our computational fluid model start from the straight segment to form a smooth transition from the straight segment to the curved segment, so that the hemodynamic characteristics of the curved segment can be conducted precisely.

In order to simulate the configuration of vascular accurately, we conducted precise and detailed measurements on the anatomical data of the variant right cephalic vein together with external jugular vein, the abnormal drainage in this case. According to the configuration features, the variant cephalic vein was divided into 5 segments from the midpoint of the right arm to the end of the cephalic vein draining into the right external jugular vein: straight segment, planar curved segment, convex segment, segment anterior to clavicle, and segment superior to clavicle. The segmentation of the variant cephalic vein and measurement of anatomical parameters were strated from the midpoint of the arm to provide morphological information for 3D computational modeling, as the modeling starts from the midpoint of the arm. Rather than using existing anatomical segmentation of the cephalic vein, the segmentation in our present study is customized which is completely based on the configuration of the blood vessels to adapt to 3D computational modeling.

Due to the fact that the high-velocity blood in the variant cephalic vein of arteriovenous fistula flow through the external jugular vein to drain into the subclavian vein, we also measured and calculated the anatomical data of the external jugular vein related to the variant cephalic vein, in order to provide sufficient information for 3D computational modeling. We integrated morphological data of

5

external jungular vein and variant cephalic vein into the 3D computational modeling system, to simulate the hemodynamic characteristics of blood returning to the subclavian vein under the special variant route of the cephalic vein in this case.

The measurement of parameters of normal right cephalic vein as a control

As a comparison for the variant cephalic vein, we conducted precise measurements on the anatomical parameters of a right normal cephalic vein to provide configuration parameters for 3D computational modeling. Due to the fact that the variant cephalic arch becomes narrow than other segments, we selected a normal running cephalic vein with narrowing of the diameter of the cephalic vein arch in order to control the metrics and prove that the differences in hemodynamics are completely caused by abnormal drainage, and compared it with the hemodynamic parameters of the variant cephalic vein for analysis. The normal cephalic vein was divided from the midpoint of the right arm to the end of the cephalic vein injecting into the right subclavian vein into three segments: straight segment, oblique segment, and cephalic arch. Starting from the midpoint of the arm, the anatomical parameters of the normal cephalic vein were measured and segmented to collect precise data for computer 3D modeling, as modeling starts from the midpoint of the arm. The segmentation of the cephalic vein described here is customized according to the shape of the blood vessels to adapt to 3D modeling, instead of using the existing anatomical segmentation of the normal cephalic vein. This segmentation method is defined completely according to the shape of the blood vessels. Computational modeling with this morphological definition will conform to the actual hemodynamics parameters of the cephalic vein under physiological conditions.

In addition, we took pictures in the sagittal plane, coronal plane and cross sections of the variant and normal cephalic vein, so as to obtain the bending angle of the blood vessels on the pictures. In order to ensure that the angle of the photo coincides with the Cartesian coordinate system used in computational modeling, we used the level function when taking photos. Every photo included the vessel and a

10.00 mm vernier caliper next to the blood vessel as a scale, so that length data can be calculated proportionally on the image.

Software used in this study

Adobe Photoshop 2022 (RRID:SCR_014199) was used to process images. To acquire morphological data that cannot directly measured, the photo of vessel can be imported into Photoshop and measured on computer.

AutoCAD 2021 (Autodesk, San Francisco, CA, RRID: SCR_021072) is a computer-aided design software used for three-dimensional modeling. Based on morphological data, the software can be used to build the geometry accurately to represent the segment of corresponding blood vessels.

COMSOL Multiphysics 5.6 (Stockholm, Sweden, RRID: SCR_014767) is one of the powerful CFD tool. After setting the boundary conditions and inherent physical characteristics of the fluid, the software can simulate blood flow based on real-world processes. As a software for finite element analysis, COMSOL can discretizing the geometry with meshes and solve the Navier-Stokes equation at any element of the model. By using COMSOL, we can analyse hemodynamic environment and calculate some parameters of blood flow.

Anatomical data processing and 3D reconstruction of the cephalic arch

In addition to the data measured directly on the cadaver specimen, we also need data for 3D reconstruction, such as the direction and angle of blood vessel bending, which needs to be further processed on the photos. Anatomical data were processed by Photoshop. According to segment of cephalic vein setting previously, we plotted segmented straight lines on the photos along the blood vessels. Then the length on photos and angle data of the variant vein can be obtained in the shape property. In photos with 10.00 mm vernier caliper, we drew a straight line between the two feet of the vernier caliper and obtained the length measured in the photo. Then we can know how long the actual 10 mm in picture for reference. According to the scaleplate, we can calculate the actual length of each segment in reality by the same scale. For each

segment, we took at least two pictures in mutually perpendicular planes for the data measurement and processing, and take the average value of the length of the same segment.

After processing the anatomical parameter exactly, we used AutoCAD to perform the 1:1 scale 3D computational model of the variant jugulocephalic vein together with the draining external jugular vein to represent geometrical characters of the variant cephalic arch precisely [10]. According to the shape parameters of each segment, we constructed a spline as the backbone of variant vein on the top view, and each anchor points on the spline were based on the junction points of adjacent vessel segments and extreme point of blood vessel. After establishing the plane model of the backbone, we shift to the left view to adjust the longitudinal bending and curve of the spline. According to the data extracted from photos on the left side and top view, we constructed the geometric solid structure of the spline to obtain the three-dimensional model of the backbone of the variant vein.

In order to study the blood flow direction and reflux situation of the abnormal drainage system, in addition to the variant cephalic vein, we established a 3D computational model of the external jugular vein together with its tributaries. In order to control the boundary conditions at the end of the blood vessels, the transverse jugular vein, supraclavicular vein, and anterior jugular vein were extended in a straight line of 1 cm according to the relative position and direction between the real blood vessels.

Boundary and initial conditions

Blood flow parameters in the arteriovenous fistula was used as the boundary condition to simulate the hemodynamic environment in the computational fluid model of the variant vein. Thus the blood flow environment and various hemodynamic parameters can be simulated in the venous outflow tract during the initial construction of the arteriovenous fistula. Based on these results, our present study further investigated the possible consequences of the maturation process of the arteriovenous

fistula with the variant vein as the outlet. In order to establish a comparison with the hemodynamics of the variant cephalic vein, the initial conditions used for modeling the normal cephalic vein were the same as those of the variant cephalic vein.

As boundary conditions, blood was assumed as non-Newtonian fluid with Carreau rheological model based on actual blood analysis data [8] and blood density was considered as 1.045 g/cm^3. With no-slip boundary condition, blood vessel walls were considered to be rigid. The direction of gravity was set to be positive along the y-axis to simulate the hemodynamic characteristics of the variant cephalic arch in upright position. The inlet of our model is located at midpoint of arm on cephalic vein, with velocity of 0.9045 m/s. The main outlet of our model is the end of external jugular vein, and the total pressure was set as 2666 Pa. In the model of variant cephalic vein draining into the external jugular vein, the external jugular vein had 4 tributaries, so the entrances of these tributaries were set as additional outlets, with total pressure of 1599 Pa.

Computational fluid dynamics model

Based on the 3D geometrical model, we simulated blood flow field with CFD package inside COMSOL, the software for multiphysics simulation. After importing the 3D geometrical model into the system, our present study was defined as steady-state study of the laminar flow model. The idealized vascular model was processed with fillets and feature repair to make the geometric modeling closer to the true vascular shape, ensure that the blood flow model remains smooth, and reduce the non-convergent site. After forming a union of all geometric elements, define the boundary conditions of the fluid.

Then we built the grid onto the simulating fluent model using computational method to discretize the model into infinitesimal elements. The resulting grids of variant vessel model contained approximately 3.29 million tetrahedral elements.

After all of the simulating fluent model having been defined, we used CFD tool to solve the continuity Navier–Stokes equations numerically for single-phase blood

flow. The influent field inside the variant jugulocephalic vein can be mathematically modeled to get a detailed description of hemodynamic environment. The free degree of our present computational model is 3296712. After calculation, the flow rate, shear rate, and other hemodynamic data at each position on the computational model can be accurately read by adjusting the data range of the plot.

RESULTS

Characteristics of jugulocephalic vein variation

The variant jugulocephalic vein lies in the lateral bicepital groove. Then it ascends anterior to deltoid muscle, rather than enters the interval between deltoid and pectoralis major. 13.74 mm from the beginning of the deltoid muscle pectoralis major groove, 26.80 mm from the deltoid muscle pectoralis major groove, and 12.68 mm from the end of the deltoid muscle pectoralis major groove. The variant cephalic vein runs anterior to the clavicle and then runs superomedially to enter the descending external jugular vein in a "T" shape (Fig.1). After receiving the variant cephalic vein, the external jugular vein also receives the superficial jugular vein and two transverse jugular veins. Afterwards, the external jugular vein suddenly becomes larger. The external jugular vein also receives the anterior jugular vein just before draining into the subclavian vein, further increasing the diameter of the external jugular vein.

Parameters of right cephalic arch variation for 3D reconstruction

The length of the five segments of the variant cephalic vein from the midpoint of the right arm to the end of the cephalic vein where it drains into the right external jugular vein is 54.52 mm in a straight segment, 41.00 mm in a planar curved segment, 77.00 mm in a convex segment, 16.98 mm in the segment anterior to clavicle, and 11.34 mm in the segment superior to clavicle. The parameters used for 3D modeling of each segment of the vein are shown in Table 1. The parameters used for 3D modeling related to external jugular vein are shown in Table 2.

Parameters of normal right cephalic vein for 3D reconstruction

The normal cephalic vein from the midpoint of the right arm until the end of the cephalic vein injects into the right subclavian vein, the length of each segment is 92.56 mm in straight segment, 79.90 mm in oblique segment, and 52.66 mm in curved segment of the cephalic vein arch. The parameters used for 3D modeling of each segment of the normal cephalic vein are shown in Table 3.

Simulating flow in 3D computational model of variant cephalic arch

The special variant we found in cadaver can be encountered when creating arteriovenous fistula during hemodialysis in clinical practice. Therefore, we simulated the possible hemodynamic changes that may occur in vivo through modeling.

Alteration and distribution of wall shear stress

In the variant cephalic arch model, the wall shear rates of the straight segment $(1.602×10^3/s-1.810×10^3/s)$ and planar curved segment $(1.792×10^3/s-2.477×10^3/s)$ were lower than other segments, and the distribution of wall shear rates in these vascular segments appeared more even and steady (Fig. 2A). At the inner wall of the bend vessel, the shear rate was slightly higher, while the shear rate in straight vessel segment was lower. The contour line of shear rate roughly arranged as parallel circular form, indicating stable hemodynamic environment in these segments. From convex segment, the wall shear stress $(1.775×10^3/s -4.686×10^3/s)$ began to rise gradually. To shows the distribution and alterations of wall shear rate in variant cephalic vein in multiple direction of view, an animation was provided as Supplement data 1.

The isopleth of shear rate in vessel segments anterior and superior to clavicle significantly became denser and crowded, indicating the shear rate changed rapidly. The wall shear rate in segments anterior and superior to clavicle continued to increase, without any areas where the shear rate decreased. The contour lines of wall shear rate in segment anterior to clavicle were arranged in a circular shape, indicating that the hemodynamic characteristics were still relatively stable in this segment. As the position became closer to the confluence, the isopleth of shear rate became denser,

which means the change of wall shear stress became faster. The wall shear rate at the end of the segment anterior to clavicle reached to 1.651×10^4/s. The shear rate in segment superior to clavicle increased sharply, and the contour spacing narrows. The maximum wall shear rate was 2.599×10^4/s, which appeared at the confluence in the inferior wall of the cephalic vein. It is worth noting that the contour around the confluence at the end of the segment superior to clavicle became disordered, and the shear rate ranged from 2.460×10^4/s to 2.599×10^4/s. In a distance of 11.34 mm, the wall shear rate of segment superior to clavicle increased for 9.48×10^3/s, indicating a rapid increase in this segment (Fig. 2C, D).

After the blood flow in variant cephalic vein drained into the external jugular vein, the local wall shear stress was disorder. The isopleth in the wall of external jugular vein at the level of the cephalic vein confluence formed a band-shaped area with low shear rate. The shear rate in this area changed rapidly, which appeared that the isoplethes were extremely dense, and the shear rate ranged from 45/s to 329.9/s. There were elliptical high shear rate regions above and below this low shear rate band. The shear rate at the periphery of the high shear rate zone above was 329.9/s, and the closer it was to the center, the higher the shear stress, with a maximum of 445.8/s at the center. The shear rate in the high shear rate zone inferior to the low shear rate band was lower than that in the upper zone, with a peripheral shear rate of 236.3/s and a maximum of 397.1/s at the center. A circular high shear rate zone was formed around the entrance of the cephalic vein, with a circular low shear rate zone above and below each, with a minimum shear rate of 15.40/s. The shear rate contour lines in the vicinity arranged in a circular pattern around these areas (Fig. 2E). Generally, the wall shear rate environment of the external jugular vein near the entrance of the cephalic vein was complex, and the hemodynamics was unstable. After crossing this area, the wall shear rate of the external jugular vein gradually decrease and tend to stable.

On the contour map of shear rate, we marked the abnormal wall shear stress areas (below 0.076 Pa and above 40 Pa) [5]. The higher wall shear stress appeared at

the end of the segment anterior to clavicle and segment superior to clavicle (Fig. 3A, C, D). The wall shear stress of the small tributaries of external jugular vein was not included in this study. There was no area with low wall shear stress on the cephalic vein to external jugular vein reflux pathway. The shear stress on the wall of the external jugular vein at the injection site of the cephalic vein changed rapidly, and the hemodynamic environment was complex, but it was still within the normal range of wall shear stress.

Velocity profile and streamline image

After the blood flow in variant cephalic vein drained into the external jugular vein, the diameter of the blood vessel suddenly becomes larger, and the high-speed blood flow in the outlet vein of arteriovenous fistula shunted upward and downward,

On the velocity profile and streamline image, it can be observed that the full length streamline of the cephalic vein was basically parallel to the tube wall, and flowed against the lower side of the tube wall under the action of gravity. The flow velocity in the straight, planar curved, and convex segments was lower, and gradually increased in the segment anterior to clavicle. The flow velocity reached to the highest in the segment superior to clavicle (Fig. 4A). From the serial sections along the yz plane of this segment, the highest velocity existed in the central part of the flow (Fig. 4E). The blood flow in the straight and curved segments was stable, and the flow velocity did not exceed 1.5 m/s. The flow velocity in the convex segment slightly increased, with a maximum flow velocity of 2.31 m/s at the end of this segment. The flow velocity in the segment anterior to clavicle sharply increased (increase of 2.16 m/s at a distance of 16.98 mm), with a maximum flow velocity of 4.47 m/s at the end of this segment. The flow velocity in the segment superior to clavicle continued to increase rapidly, reaching the highest velocity of 6.34 m/s at the center of the injection site (Fig. 4D, E).

After injection into the external jugular vein, the high-speed flow of arteriovenous fistula blood did not immediately flow axially along the wall of the

external jugular vein. Instead, it still flowed in the same direction of the end of the cephalic vein with a speed of 4.81 m/s to the lumen center of the external jugular vein sharply decreased to 0.64 m/s (Fig. 4C, D, E). Then, the flow began to upwards (0.25 m/s) and downwards (0.20 m/s) along with the external jugular vein axis. The upstream of this abnormal flow in this variant may cause obstruction of the external jugular vein reflux, which may cause congestion and edema in the head and neck. Furthermore, local turbulence or even vortex was formed downward, which disturbed local venous blood flow and may cause local thrombosis and endothelial damage (Fig. 4D). Other abnormal flow may exist at the junction between superficial jugular vein and external jugular vein (Fig. 4C), which may cause congestion, edema, and pain in the drainage area of the superficial jugular vein. The other tributaries of the external jugular vein, including the superior and inferior branches of the transverse jugular vein and the anterior jugular vein, did not have abnormal blood flow. It is suggested that the abnormal hemodynamic characteristics of arteriovenous fistulas caused by variant cephalic veins may cause local venous reflux disorders, but did not affect the veins in the entire blood reflux pathway. After receiving blood from the inferior branch of the transverse jugular vein, the blood flow velocity of the external jugular vein did not exceed 0.1 m/s, and the blood flow velocity returned to normal. The velocity alterations of variant cephalic vein in multiple direction of view were shown as an animation in Supplement data 2.

Range and distribution of vortex intensity

The vector reflecting eddy current intensity was represented by solid arrows which arranged with right-hand spiral direction around the wall of the blood vessel. The eddy current vector was perpendicular and right-hand spiral direction to the blood flow (Fig. 5D). The vortex intensity in the center of the blood vessel was relatively small, while the vortex intensity near the wall of the blood vessel was relatively large. The eddy current intensity gradually increased from the straight segment and reached to the highest point at the end of the segment superior to clavicle (Fig. 5A). The eddy

current value of the straight segment, planar curved segment, and convex segment did not exceed $5×10^3$/s, indicating that the blood flow in these segments was stable and less eddy current formation. The eddy current intensity in the segment anterior to clavicle begins to rise, and the eddy current value did not exceed $1.5×10^4$/s at the end of this segment. The eddy current intensity reached to the highest point as $1.59×10^5$/s at the end of segment superior to clavicle (Fig. 5C, D). In the external jugular vein, the eddy current intensity sharply decreased near to the "T-junction" and tended to zero peripherally. The vortex intensity in variant cephalic vein in multiple direction of view was shown as an animation in Supplement data 3.

Comparison of this variation with normal cephalic arch

The shear rate of variant cephalic vein was higher than that in normal cephalic vein at corresponding part. The highest shear rate in the variant cephalic vein $(2.599×10^4$/s) was much higher than that in the normal cephalic vein $(1.67×10^4$/s), which existed at the narrowest part of the veins (Fig.2A, B). In addition, the dense circular contour lines around variant cephalic vein showed that the wall shear rate in the variant cephalic vein changes much more rapidly than that in the normal cephalic vein. Only variant cephalic vein exhibited abnormal reflux, multi-direction blood flow, and vortex as shown in the streamline image (Fig. 4A, B) The shear rate in external jugular vein in this variant case was much more complex for its abnormal drainage.

Overall, from the 3D computational model of variant cephalic arch, we found that compared with the normal cephalic arch, the unsteady turbulent flow and multi-directional flow appeared in the variant cephalic arch, forming several large regions with pathological flow patterns and higher gradients of wall shear stress on the variant vein (Fig. 5A, B). Disturbed flow may induce pathological wall shear stress environment, which stimulated venous endothelial cells in variant cephalic arch and prone to induce intimal hyperplasia and vascular stenosis. Therefore, the variant cephalic vein arch is prone to stenosis during remodeling and maturation after

brachiocephalic fistula.

DISCUSSION

Simulating the hemodynamic changes of variant cephalic vein is not only of great theoretical significance, but also of great clinical significance correlation with the management of brachiocephalic fistula. Here, we simulated the flow in 3D computational model of "T-junction" single-conduit supraclavicular cephalic arch draining into the external jugular vein variant after brachiocephalic fistula. The results of our present study showed that: (1) the variation of cephalic arch in the "T-junction" with external jugular vein largely altered the fluid dynamics, especially in patients with brachiocephalic fistula; (2) this single-conduit supraclavicular cephalic arch draining into the external jugular vein is prone to form stenosis after brachiocephalic fistula; (3) the mechanism of stenosis of the single-conduit supraclavicular cephalic arch variant after brachiocephalic fistula might be that more flow disturbances in variant vein have pro-inflammatory effect from the simulating flow in 3D computational model. This simulating flow in 3D computational model explained the mechanism of stenosis of the single-conduit supraclavicular cephalic arch variant after brachiocephalic fistula and paved the way for further investigating the different variants of cephalic arch and developing anatomical based therapeutic interventions after brachiocephalic fistula.

The factors causing damage to the variant cephalic vein and the potentially problematic areas in the vein were found through our analysis of the 3D computational model based on this "T-junction" single-conduit supraclavicular cephalic arch draining into the external jugular vein. Vortex formation is one of the harmful factors to the vein used for anastomosis. The cause of vortex formation is the local adverse pressure gradient of blood flow [3]. On the inner side of the tight bend of blood vessel, the sharp turn of the direction is prone to form local adverse pressure gradient of blood flow, which lead to local reverse flow [17]. Thus, vortices appeared in many separate areas in the bend of the vessel. In this variant case,

the "T-junction" end of the cephalic vein draining into the external jugular vein is prone to form obvious vortices comparison with the normal cephalic vein draining into the axillary or subclavian vein. The course of the cephalic arch changed obviously in this variant, which passes anterior to the clavicle. The extrinsic compression by the underlying clavicle bone may contribute to the formation of vortex. The external jugular vein received several tributaries adjacent to the end of the cephalic vein. Hence, there is a possibility that the blood of the cephalic vein can flow into these tributaries upon the increased pressure after brachiocephalic fistula. All the above harmful factors complicated the hemodynamics in this specific variant cephalic arch after brachiocephalic fistula.

Upon the establishment of brachiocephalic fistula, the blood pressure in the vein suddenly increases, leading to an increased Reynolds number with its flow pattern converting from laminar to a disturbed one. The artificially established fistula alters the hemodynamics of the variant cephalic arch, exposing venous endothelial cells to a supra-physiological shear force [21], where the wall shear stress was below 0.076 Pa or above 40 Pa. To normalize wall shear stress and maintain vasculature homeostasis, the brachiocephalic fistula should undergo extensive vascular remodeling [6]. In this situation, the shear stress below normal level (<0.076 Pa) laterally impacts the vascular wall, which activates endothelial cells and potentially trigger inflammatory response. These pathological responses of the variant vein can leads to reactive proliferation of vascular muscle and neointimal hyperplasia [7]. The shear stress exceeding normal range (>40 Pa) causes endothelial denudation which result in the hemodynamic insult on the vascular wall. These two factors (abnormal lower or higher wall shear stress) are the main reason of non-uniform remodeling and non-maturation of arteriovenous fistula [18]. On the other hand, the low vortex area is easily to the deposition of lipids and blood cells, resulting in the formation of early thrombosis, which further aggravates the degree of hemodynamic abnormalities. Above factors may provide possible nidus that lead to stenosis and thrombosis. Analyzing the key factors affecting stenosis, solving the complex pathogenesis, and

searching the effective measures to eliminate the harmful factors on stenosis might be attractive research directions.

In view of the complexity of hemodynamics after this variant brachiocephalic fistula for this "T-junction" single-conduit supraclavicular cephalic arch draining into the external jugular vein, the surgeons should pay attention to the following important issues during the clinical practice: The harmful factors of this cephalic vein variant during and after brachiocephalic fistula should be preliminary evaluated. The relevant clinical parameters should be monitored whenever necessary after brachiocephalic fistula [16]. Once the pulsatile flow disappeared at the site of brachiocephalic fistula, the effective measures should be taken to avoid severe adverse effects [13]. Nowadays, color Doppler is the main method for evaluation of brachiocephalic fistula maturation [22]. By using the computational modeling technique, we can predict the high-risk region after creation of brachiocephalic fistula and take measure to prevent maturation-failure in time [9,15].

Because of complexity of hemodynamic environment in brachiocephalic fistula, computational modeling is widely used for hemodynamic study of brachiocephalic fistula [1]. In intravital cases, these hemodynamic studies often use ultrasound or CT for hemodynamic simulating. Compared with the two-dimensional modeling, the 3D model can comprehensively simulate the hemodynamic changes in the blood vessels with complex courses, complicated configuration, and irregular connections with other vessels. A larger amount of hemodynamic parameters can be investigated theoretically. These advantages will contribute to access the realistic situation before and after brachiocephalic fistula. Although the model established in this study cannot precisely simulate the complicated blood flow in this variant cephalic arch after brachiocephalic fistula, the new viewpoints raised in our present study paves the way for further detailed investigation in this specific field.

Limitations of the study

Instead of reconstruction of imaging data, the geometrical model in our present

study is build by computer-aid design software which was based on data from specimens. So it may have some bias compared to the reconstruction of real imaging data. However for cadaver, it is difficult to obtain imaging data. Computational simulations of hemodynamic changes can be used as an explanation for this specific state of variation.

The selection of boundary conditions is based on a reasonable range of normal values. The real data of velocity, viscosity and pressure can be measured in vivo, which cannot be obtained on cadaver specimens.

CONCLUSIONS

The results from the simulating flow in 3D computational model support the view that the variation of cephalic arch in a "T-junction" with external jugular vein largely altered the fluid dynamics, especially in hemodialysis patients with brachiocephalic fistula. This computational model underpins the concept that a regular management of hemodynamic profiles in patients with jugulocephalic vein variant after brachiocephalic fistula may help stabilize or modulate fluid dynamics in this specific situation.

Conflicts of interest: None declared

References

1. Alam N, Walsh M, Newport D (2022) Experimental evaluation of a patient specific Brachio-Cephalic Arterio Venous Fistula (AVF): Velocity flow conditions under steady and pulsatile waveforms. Med Eng Phys 106: 103834. doi: 10.1016/j.medengphy.2022.103834.

2. Araújo RC, Pires LAS, Andrade ML, Perez MC, Filho CSL, Babinski MA (2018) Embryological and comparative description of the cephalic vein joining the external jugular vein: A case report. Morphologie 102(336): 44-47. doi: 10.1016/j.morpho.2017.10.002.

3. Bai H, Sadaghianloo N, Gorecka J, Liu S, Ono S, Ramachandra AB, Bonnet S, Mazure NM, Declemy S, Humphrey JD, Dardik A (2020) Artery to vein configuration of arteriovenous fistula improves hemodynamics to increase maturation and patency. Sci Transl Med 12(557): eaax761. doi: 10.1126/scitranslmed.aax7613.

4. Beathard GA, Jennings WC, Wasse H, Shenoy S, Falk A, Urbanes A, Ross J, Nassar G, Hentschel DM, Sachdeva B, Chan MR, Salman L, Asif A (2023) ASDIN white paper: Management of cephalic arch stenosis endorsed by the American Society of Diagnostic and Interventional Nephrology. J Vasc Access 24(3): 358-369. doi: 10.1177/11297298211033519.

5. Boghosian M, Cassel K, Hammes M, Funaki B, Kim S, Qian X, Wang X, Dhar P, Hines J (2014) Hemodynamics in the cephalic arch of a brachiocephalic fistula. Med Eng Phys 36(7): 822-830. doi: 10.1016/j.medengphy.2014.03.001.

6. Colley E, Simmons A, Varcoe R, Thomas S, Barber T (2020) Arteriovenous fistula maturation and the influence of fluid dynamics. Proc Inst Mech Eng H 234(11): 1197-1208. doi: 10.1177/0954411920926077.

7. Corretti MC, Anderson TJ, Benjamin EJ, Celermajer D, Charbonneau F, Creager MA, Deanfield J, Drexler H, Gerhard-Herman M, Herrington D, Vallance P, Vita J, Vogel R; International Brachial Artery Reactivity Task Force (2002) Guidelines

for the ultrasound assessment of endothelial-dependent flow-mediated vasodilation of the brachial artery: a report of the International Brachial Artery Reactivity Task Force. J Am Coll Cardiol 39(2): 257-265. doi: 10.1016/s0735-1097(01)01746-6.

8. Ene-Iordache B, Mosconi L, Remuzzi G, Remuzzi A (2001) Computational fluid dynamics of a vascular access case for hemodialysis. J Biomech Eng 123(3): 284-292. doi: 10.1115/1.1372702.

9. Franco G, Mallios A, Bourquelot P, Jennings W, Boura B (2020) Ultrasound evaluation of percutaneously created arteriovenous fistulae between radial artery and perforating vein at the elbow. J Vasc Access 21(5): 694-700. doi: 10.1177/1129729819897654.

10. Hammes M, Moya-Rodriguez A, Bernstein C, Nathan S, Navuluri R, Basu A (2021) Computational modeling of the cephalic arch predicts hemodynamic profiles in patients with brachiocephalic fistula access receiving hemodialysis. PLoS One 16(7): e025401. doi: 10.1371/journal.pone.0254016.

11. Jun ESW, Lun ALY, Nikam M (2017) A rare anatomic variant of a single-conduit supraclavicular cephalic arch draining into the external jugular vein presenting with recurrent arteriovenous fistula stenosis in a hemodialysis patient. J Vasc Surg Cases Innov Tech 3(1): 20-22. doi: 10.1016/j.jvscit.2016.12.001.

12. Kameda S, Tanaka O, Terayama H, Kanazawa T, Sakamoto R, Tetsu S, Sakabe K (2018) Variations of the cephalic vein anterior to the clavicle in humans. Folia Morphol (Warsz) 77(4): 677-682. doi: 10.5603/FM.a2018.0018.

13. Kim HK, Han A, Ahn S, Ko H, Chung CTY, Choi KW, Min S, Ha J, Min SK (2021) Better efficacy of balloon assisted maturation in radial-cephalic arteriovenous fistula for hemodialysis. Vasc Specialist Int 37(1): 29-36. doi: 10.5758/vsi.210003.

14. Lee HN, Yang SB, Lee WH, Cho Y, Park SJ, Lee S (2022) Prevalence and clinical significance of anatomic variant in cephalic arch on preoperative mapping venography. Sci Rep 12(1): 17398. doi: 10.1038/s41598-022-22372-0.

15. Moya-Rodríguez A, Xie B, Cook D, Klineberg M, Nathan S, Hammes M, Basu A

(2022) Creating patient-specific vein models to characterize wall shear stress in hemodialysis population. Comput Struct Biotechnol J 20: 5729-5739. doi: 10.1016/j.csbj.2022.10.010.

16. Pirozzi N, Mancianti N, Scrivano J, Fazzari L, Pirozzi R, Tozzi M (2021) Monitoring the patient following radio-cephalic arteriovenous fistula creation: Current perspectives. Vasc Health Risk Manag 17: 111-121. doi: 10.2147/VHRM.S205130.

17. Prouse G, Stella S, Vergara C, Quarteroni A, Engelberger S, Canevascini R, Giovannacci L (2020) Computational analysis of turbulent hemodynamics in radiocephalic arteriovenous fistulas to determine the best anastomotic angles. Ann Vasc Surg 68: 451-459. doi: 10.1016/j.avsg.2020.04.004.

18. Remuzzi A, Ene-Iordache B, Mosconi L, Bruno S, Anghileri A, Antiga L, Remuzzi G (2003) Radial artery wall shear stress evaluation in patients with arteriovenous fistula for hemodialysis access. Biorheology 40(1-3): 423-430.

19. Soliveri L, Bozzetto M, Brambilla P, Caroli A, Remuzzi A. Hemodynamics in AVF over time: A protective role of vascular remodeling toward flow stabilization. Int J Artif Organs. 2023 Sep 27: 3913988231191960. doi: 10.1177/03913988231191960.

20. Xiao Y, Martinez L, Zigmond Z, Woltmann D, Singer DV, Singer HA, Vazquez-Padron RI, Salman LH. Functions for platelet factor 4 (PF4/CXCL4) and its receptors in fibroblast-myofibroblast transition and fibrotic failure of arteriovenous fistulas (AVFs). J Vasc Access. 2023 Aug 17: 11297298231192386. doi: 10.1177/11297298231192386.

21. Yang CY, Li MC, Lan CW, Lee WJ, Lee CJ, Wu CH, Tang JM, Niu YY, Lin YP, Shiu YT, Cheung AK, Lee YW, Lee OK, Chien S, Tarng DC (2020) The anastomotic angle of hemodialysis arteriovenous fistula is associated with flow disturbance at the venous stenosis location on angiography. Front Bioeng Biotechnol 8: 846. doi: 10.3389/fbioe.2020.00846.

22. Yun SS, Mok S, Park SC, Park YJ, Kim JY (2023) Efficacy of blood flow measurement using intraoperative color flow Doppler ultrasound as a predictor of

autologous arteriovenous fistula maturation. Ther Apher Dial 27(1): 50-58. doi: 10.1111/1744-9987.13855.

23. Zhu Y, Xu XY, Mason J, Mirsadraee S. Irregular anatomical features can alter hemodynamics in Takayasu arteritis. JVS Vasc Sci. 2023 Aug 24; 4: 100125. doi: 10.1016/j.jvssci.2023.100125.

Table 1. The parameters used for 3D modeling of each segment of the variant cephalic vein

Length and diameter parameters	[mm]	Angle parameters	Angle
Diameter at beginning of straight segment	0.97	[1]Angle between straight segment and vertical axis	-8°
Length of straight segment	54.52	[2]Anteversion angle of straight segment	10°
Diameter at beginning of planar curved segment	1.11	[3]Angle between chord of planar curved segment and vertical axis	29°
Chord length of planar curved segment	68.88	Anteversion angle of chord of planar curved segment	24°
Diameter at beginning of convex segment	1.10	Angle between convex segment and vertical axis	54°
Length of convex segment	77.00	Anteversion angle of convex segment	26°
Diameter at beginning of segment anterior to clavicle	0.89	Angle between segment anterior to clavicle and vertical axis	46°
Length of segment anterior to clavicle	16.98	[4]Posterior inclination angle of segment anterior to clavicle	29°
Diameter at beginning of the segment superior to clavicle	0.75	Angle between segment superior to clavicle and vertical axis	69°
Length of the segment superior to clavicle	11.34	Posterior inclination angle of segment superior to clavicle	29°
Diameter at the end of the segment superior to clavicle	0.51		

[1]Angle between straight segment and vertical axis: The straight segment inclined to right side was defined as negative number (-8°). [2]Anteversion angle of straight segment: The angle of straight segment anterior to vertical axis. [3]Angle between chord of planar curved segment and vertical axis: The chord of planar curved segment inclined to left side was defined as positive number (29°). [4]Posterior inclination angle of segment anterior to clavicle: The angle of segment anterior to clavicle posterior to vertical axis.

Table 2. The parameters of external jugular vein used for 3D modeling

Length and diameter parameters	[mm]	Angle parameters	Angle
Diameter at beginning of external jugular vein	1.80	Angle between external jugular vein before superficial cervical vein joining and vertical axis	0°
Diameter of external jugular vein after joining cephalic vein	1.80	Posterior inclination angle of external jugular vein before superficial cervical vein joining	47°
Distance between joining sites of cephalic vein and superficial cervical vein	8.26	[1]Angle between superficial cervical vein and vertical axis	60°
Diameter of superficial cervical vein	1.82	Posterior inclination angle of superficial cervical vein	73°
Diameter of external jugular vein after joining superficial cervical vein	2.59	[2]Angle between transverse cervical vein and vertical axis	-74°
Distance between joining sites of superficial jugular vein and superior branch of transverse cervical vein	9.60	Anteversion angle of transverse cervical vein	41°
Diameter of superior branch of transverse cervical vein	1.97	Angle between the segment of external jugular vein from superior transverse cervical vein to the inferior transverse cervical vein and vertical axis	59°
Distance between joining sites of superior and inferior branch of transverse cervical vein	6.26	Posterior inclination angle of the segment of external jugular vein from superior transverse cervical vein to the inferior transverse cervical vein	29°
Diameter of inferior branch of transverse cervical vein	2.24	Angle between the segment of external jugular vein inferior to clavicle and vertical axis	68°
Distance between joining sites of inferior branch of transverse cervical vein and anterior jugular vein	45.70	Posterior inclination angle of external jugular vein inferior to clavicle	57°
Diameter of external jugular vein after joining inferior branch of transverse cervical vein	3.22	Angle between of anterior jugular vein and vertical axis	-83°
Diameter of anterior jugular vein	3.03	Posterior inclination angle of anterior jugular vein	73°

Diameter of external jugular vein after joining anterior jugular vein	4.38		
Distance between joining sites of anterior jugular vein and the end of external jugular vein	17.44		
Diameter of the end of external jugular vein	4.38		

[1]Angle between superficial cervical vein and vertical axis: The superficial cervical vein inclined to right side was defined as positive number (60°). [2]Angle between transverse cervical vein and vertical axis: The transverse cervical vein inclined to left side was defined as negative number (-74°).

Table 3. The parameters used for 3D modeling of each segment of the normal cephalic vein

Length and diameter parameters	[mm]	Angle parameters	Angle
Diameter at beginning of straight segment	2.11	[1]Angle between straight segment and vertical axis	-7°
Length of straight segment	92.56	Posterior inclination angle of straight segment	1°
Diameter at beginning of oblique segment	2.16	[2]Angle between oblique segment and vertical axis	30°
Length of oblique segment	99.90	Posterior inclination angle of oblique segment	10°
Diameter at beginning of cephalic arch	1.82	Angle between the line from the beginning to the highest point of cephalic arch and vertical axis	42°
Distance between the beginning and the highest point of cephalic arch	37.75	Posterior inclination angle of the line from the beginning to the highest point of cephalic arch	26°
Diameter of the highest point of cephalic arch	1.11	Angle between the line from the highest point to the end of cephalic arch and vertical axis	-63°
Distance between the highest point of cephalic arch and the joining point	42.36	Posterior inclination angle of line from the highest point the end of cephalic arch	51°
Diameter of cephalic arch at	1.99		

the joining point

[1]Angle between straight segment and vertical axis: The straight segment inclined to right side was defined as negative number (-7°). [2]Angle between oblique segment and vertical axis: The oblique segment inclined to left side was defined as positive number (30°).

Figure 1. Comparison of cephalic vein draining into external jugular vein with "T-junction" shape variation and normal cephalic vein. **A** Cephalic vein draining into external jugular vein with "T-junction" shape variation in a cadaver. **B** Normal cephalic vein in a cadaver. **C** Illustration for cephalic vein draining into external jugular vein with "T-junction" shape variation. **D** Illustration for normal cephalic vein.

Figure 2. The isopleth of wall shear rate in variant cephalic vein and normal cephalic vein. **A** The distribution and alterations of isopleth of wall shear rate in the model of variant cephalic vein and external jugular vein. This model was showed in XY plane with contour lines defined at 100 lines. **B** The distribution and alterations of isopleth of wall shear rate in the model of normal cephalic vein. This model was showed in XY plane with contour lines defined at 100 lines. **C** Enlargement of the box in **A**, which shows the isopleth of "T-junction". The contour lines range from 100 to 26000 with intervals as 200. **D** The same parameters of **C** at lateral side. **E** Median side of **C** with parameters of contour lines range from 0 to 450 with intervals as 10.

Figure 3. The comparison of abnormal wall shear stress region between variant cephalic vein and normal cephalic vein. **A** The abnormal wall shear stress region in variant cephalic vein. In XY plane of this model, abnormally higher wall shear stress region range from 13333 to 26700 with intervals as 200. Abnormally lower wall shear stress region range from 0 to 25.33 with intervals as 1. **B** The abnormal wall shear stress region in normal cephalic vein. Only abnormally higher wall shear stress region exists at the turn of the cephalic arch, which ranges from 13333 to 15700 with

intervals as 200. **C** Enlargement of the box in **A**, which shows the abnormally higher wall shear stress region in the terminal segment of the variant cephalic vein. The contour lines range from 13333 to 26700 with intervals as 200. **D** The same parameters of **C** at lateral side. **E** Enlargement of the box in **B**, which shows the abnormally higher wall shear stress region in the cephalic arch.

Figure 4. The comparison of streamline image between variant cephalic vein and normal cephalic vein. **A** The streamline image in variant cephalic vein. In XY plane of this model, the color shows the range of velocity from lower to higher. **B** The streamline image in normal cephalic vein. **C** Enlargement of the box in **A**, showing the transverse flow in the external jugular vein at "T-junction". The velocity alterations in the external jugular vein at "T-junction" with serial sections at XY plane. **D** The vortex in the external jugular vein at "T-junction" at lateral side. **E** The velocity alterations in the segment superior to clavicle with serial sections at YZ plane.

Figure 5. The comparison of vortex intensity between variant cephalic vein and normal cephalic vein. **A** The vortex intensity in variant cephalic vein. In XY plane of this model, the color shows the range of intensity from lower to higher. The color arrows show the vortex intensity and direction. **B** The vortex intensity in normal cephalic vein. **C** Enlargement of the box in **A**. **D** The same parameters of **C** at lateral side. **E** Enlargement of the box in **B**.

A

external jugular v.

clavicle

the variant jugulocephalic v.

deltopectoral groove
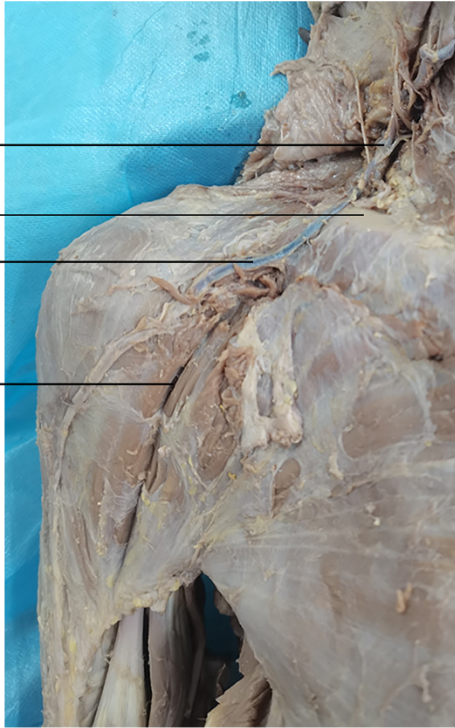
B

deltopectoral groove

cephalic v.

C

internal jugular v.

external jugular v.
superficial cervical v.

superior branch of transverse cervical v.

inferior branch of transverse cervical v.

the variant jugulocephalic v.

deltopectoral groove

basilic v.

anterior jugular v.

subclavian v.
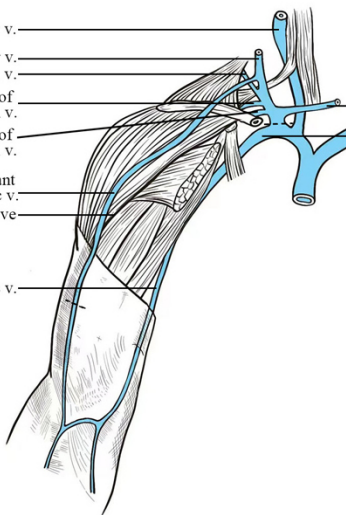
D

internal jugular v.

external jugular v.

subclavian v.

superficial cervical v.

transverse cervical v.

cephalic v.

deltopectoral groove

basilic v.

A

segment superior to clavicle
segment anterior to clavicle
external jugular v.
convex segment
planar curved segment
straight segment

▲ 3.63×10⁴
×10⁴
3.52
3.38
3.23
3.08
2.94
2.79
2.65
2.5
2.35
2.21
2.06
1.92
1.77
1.62
1.48
1.33
1.19
1.04
0.89
0.75
0.6
0.46
0.31
0.16
0.02
▼ 183

B

-5
0.05
0.1
cephalic arch
oblique segment
straight segment

0.05
0
-0.05
m

▲ 1.67×10⁴
×10⁴
1.62
1.55
1.49
1.42
1.36
1.29
1.23
1.16
1.09
1.03
0.96
0.9
0.83
0.77
0.7
0.64
0.57
0.5
0.44
0.37
0.31
0.24
0.18
0.11
0.05
▼ 453

C

external jugular v.
segment superior to clavicle
superficial cervical v.
superior branch of transverse cervical v.
inferior branch of transverse cervical v.

▲ 2.59×10⁴
×10⁴
2.51
2.41
2.31
2.21
2.11
2.01
1.91
1.81
1.71
1.61
1.51
1.41
1.31
1.21
1.11
1.01
0.91
0.81
0.71
0.61
0.51
0.41
0.31
0.21
0.11
0.01
▼ 100

D

external jugular v.
segment superior to clavicle
superficial cervical v.
superior branch of transverse cervical v.

E

external jugular v.
segment superior to clavicle
superficial cervical v.
superior branch of transverse cervical v.
inferior branch of transverse cervical v.

▲ 450
440
420
400
380
360
340
320
300
280
260
240
220
200
180
160
140
120
100
80
60
40
20
0
▼ 0

A

segment superior to clavicle
segment anterior to clavicle
convex segment
planar curved segment
straight segment

▲ 3.69×10⁴
×10⁴
3.57
3.43
3.29
3.15
3.01
2.87
2.73
2.59
2.45
2.31
2.17
2.03
1.89
1.75
1.61
1.47
1.33
0
▼ 0

B

×10⁻³ m
cephalic arch
oblique segment
straight segment

×10⁴
1.57
1.51
1.45
1.39
1.33
0

C

external jugular v.
segment superior to clavicle
superficial cervical v.
superior branch of transverse cervical v.
inferior branch of transverse cervical v.

D

external jugular v.
segment superior to clavicle
superficial cervical v.
superior branch of transverse cervical v.
inferior branch of transverse cervical v.

E

cephalic arch

A

segment superior to clavicle

segment anterior to clavicle

convex segment

planar curved segment

straight segment

▲ 3.05×10⁴
×10⁴
3
2.5
2
1.5
1
0.5
▼ 0.36

▲ 1.59×10⁵
×10⁴
2.5
2
1.5
1
0.5
▼ 0.69

▲ 3.58×10⁴
×10⁴
3.5
3
2.5
2
1.5
1
0.5
▼ 0.76

B

cephalic arch

oblique segment

straight segment

▲ 1.68×10⁴
×10⁴
1.6
1.4
1.2
1
0.8
0.6
0.4
0.2
▼ 231

▲ 1.66×10⁴
×10⁴
1.6
1.4
1.2
1
0.8
0.6
0.4
0.2
▼ 14.2

▲ 1.43×10⁴
×10⁴
1.4
1.2
1
0.8
0.6
0.4
0.2
▼ 94.3

C

external jugular v.

segment superior to clavicle

superficial cervical v.

superior branch of transverse cervical v.

inferior branch of transverse cervical v.

D

external jugular v.

superficial cervical v.

segment superior to clavicle

E

cephalic arch